Higher Order Compact Schemes for the Spatial Discretization of Linear Parabolic Partial Differential Equations

E. Dhananjaya, R. Bhuvana Vijaya

Abstract: ***A system of compact schemes used, to approximate the partial derivative of Linear Parabolic Partial Differential Equations (LPPDE), on the non-boundary nodes. Euler time integration for the temporal derivative, the Crank-Nicholson (CN)scheme for the spatial derivatives and the source term are used. The higher order spatial accuracy of the developed, central difference based compact schemes for the one and two-dimensional diffusion equations are validated, by solving numerically two test problems.***

The compact scheme based calculations involve a tridiagonal matrix vector multiplication and a vector vector subtraction. The interest is to demonstrate the higher order spatial accuracy and the better rate of convergence of the solution produced using the developed compact 4^{th} ***order scheme, when compared with the same produced, using the conventional*** 2^{nd} ***order scheme. The assessment is made, in terms of the discrete*** l_2 ***or*** l_∞ ***norm of the true error of the converged numerical solution.***

Keywords: Fourth order central difference based compact schemes, spatial discretization, Linear Parabolic Partial Differential Equations, Incompressible fluid flow, Explicit Scheme, Implicit Scheme.

I. INTRODUCTION

One of the most common model equations, belonging to the class of Linear Parabolic Partial Differential Equations (LPPDE) is the diffusion or heat conduction equation. The mathematical forms in one and two dimensions are given respectively by,

$$\frac{\partial f}{\partial t} = D_1 \frac{\partial^2 f}{\partial x_1^2} + g\left(x_1, t\right) \qquad (1.1a)$$

and

$$\frac{\partial f}{\partial t} = D_1 \frac{\partial^2 f}{\partial x_1^2} + D_2 \frac{\partial^2 f}{\partial x_2^2} + g\left(x_1, x_2, t\right) \qquad (1.1b)$$

where, D_1 and D_2 are the diffusion coefficients in the x_1 and x_2 directions, respectively. $g\left(x_1, t\right)$ and $g\left(x_1, x_2, t\right)$ are the source terms of the one and two-dimensional diffusion equations, respectively [1-4]. Equation (1.1a) must be satisfied for the distance $\left|x_1\right|$ along the real line. The boundary conditions are defined, in terms of the function and/or its derivative, on the extremities of $\left|x_1\right|$, representing the boundary points. Similarly, equation (1.1b) must be satisfied for all $\left(x_1, x_2\right)$ in some region of the plane, Ω_d. The boundary conditions are defined, in terms of the function and/or its derivative on, $\partial\Omega_d$ which represents the boundary of the domain [5-6].

Importantly, in addition to the boundary condition, it is necessary to define an initial condition, in order to satisfy the well-posedness of the problem and to obtain a unique solution for these equations.

In the next two sections, the time and the spatial discretization (using the 4^{th} order compact schemes like a spatially fourth order and temporally second order fully implicit ADI method to solve the unsteady incompressible NSE using higher order Padé schemes) [7-13] of the one and two-dimensional diffusion equations and the numerical algorithms to solve, the fully discretized equations are explained. Finally in the last part of this section, the developed numerical schemes for the equations (1.1b) and (1.1b) are tested, using two test problems (one each for the one and two-dimensional parabolic model equations), subjected to appropriate initial and Dirichlet boundary conditions.

The aim of the numerical experiments is, to demonstrate the higher order spatial accuracy and the better rate of convergence of the solution produced using the developed compact scheme. Further, these solutions are compared with the same produced, using the conventional 2^{nd} order scheme[14-17]. The comparisons are made, in terms of the discrete l_2 norm of the true error.

It is worth mentioning, that the grid independence study, for the developed numerical schemes are conducted, using an optimum time step value. This particular value is determined, by comparing, the error norm behavior of the numerical solution, produced on a fine grid, using a series of time steps values. The minimum value of the time step, after which the error norm value, become independent of further reduction in the time step is chosen, as the optimum time step value.

Revised Manuscript Received on February 10, 2020.
***** Correspondence Author

E. Dhananjaya, Research Scholar, Jawaharlal Nehru Technological University Anantapur, Ananthapuramu, Andhra Pradesh-515002, India. E-mail: dhanuelisetty@gmail.com

R. Bhuvana Vijaya, Professor and Head, Department of Mathematics, Jawaharlal Nehru Technological University Anantapur, Ananthapuramu, Andhra Pradesh-515002, India.
E-mail: bhuvanavijayarachamalla@gmail.com

II. TIME DISCRETIZATION OF THE ONE AND TWO-DIMENSIONAL DIFFUSION EQUATIONS

Using the Euler time integration for the temporal derivative, the Crank-Nicholson (CN) scheme for the spatial derivatives and the source term, the time discretized form of the equations (1.1a) and (1.1b) are given respectively by,

$$f_i^{n+1} - D_1 \frac{\Delta t}{2} \frac{\partial^2 f_i^{n+1}}{\partial x_1^2} = f_i^n + D_1 \frac{\Delta t}{2} \frac{\partial^2 f_i^n}{\partial x_1^2} + \frac{\Delta t}{2}\left[g\left(x_{1i}, t\right)^{n+1} + g\left(x_{1i}, t\right)^n \right] \quad (1.2a)$$

$$f_{i,j}^{n+1} - D_1 \frac{\Delta t}{2} \frac{\partial^2 f_{i,j}^{n+1}}{\partial x_1^2} - D_2 \frac{\Delta t}{2} \frac{\partial^2 f_{i,j}^{n+1}}{\partial x_2^2} = f_{i,j}^n + D_1 \frac{\Delta t}{2} \frac{\partial^2 f_{i,j}^n}{\partial x_1^2} + D_2 \frac{\Delta t}{2} \frac{\partial^2 f_{i,j}^n}{\partial x_2^2} + \frac{\Delta t}{2}\left[g\left(x_{1i}, x_{2j}, t\right)^{n+1} + g\left(x_{1i}, x_{2j}, t\right)^n \right] \quad (1.2b)$$

Factorizing, the LHS and RHS of the equation (1.2b) leads to,

$$\left(1 - D_1 \frac{\Delta t}{2} \frac{\partial^2}{\partial x_1^2}\right)\left(1 - D_2 \frac{\Delta t}{2} \frac{\partial^2}{\partial x_2^2}\right) f_{i,j}^{n+1} = \left(1 + D_1 \frac{\Delta t}{2} \frac{\partial^2}{\partial x_1^2}\right)\left(1 + D_2 \frac{\Delta t}{2} \frac{\partial^2}{\partial x_2^2}\right) f_{i,j}^n + \frac{\Delta t}{2}\left[g\left(x_{1i}, x_{2j}, t\right)^{n+1} + g\left(x_{1i}, x_{2j}, t\right)^n \right] \quad (1.3)$$

The factorization in the equation (1.3) implicitly means an addition of the terms $D_1 \frac{\Delta t}{2} D_2 \frac{\Delta t}{2} \frac{\partial^2}{\partial x_1^2} \frac{\partial^2}{\partial x_2^2} f_{i,j}^{n+1}$ and $D_1 \frac{\Delta t}{2} D_2 \frac{\Delta t}{2} \frac{\partial^2}{\partial x_1^2} \frac{\partial^2}{\partial x_2^2} f_{i,j}^n$ to the LHS and to the RHS of the equation (1.2b), respectively. The scheme so obtained is classified, as an approximate factorization scheme. The aim behind incorporating this factorization technique is, to derive an unconditionally stable and computationally efficient compact scheme, for the two-dimensional parabolic model equation. Also, equation (1.3) will have the same second order temporal accuracy, as the CN scheme given by the equation (1.2b).

III. COMPACT SCHEMES FOR THE SPATIAL DISCRETIZATION OF THE ONE DIMENSIONAL DIFFUSION EQUATION

A system of compact schemes used, to approximate the partial derivative $\frac{\partial^2 f}{\partial x_1^2}$, only on the non-boundary nodes, at ψ_i where, $i = 1.....\left(N_{x_1} - 1\right)$ located along the one dimensional structured Cartesian uniform grid are given by,

$$f_{\psi_1}^{"} + \alpha_L f_{\psi_2}^{"} = \frac{a_L f_{\psi_0} + b_L f_{\psi_1} + c_L f_{\psi_2} + d_L f_{\psi_3} + e_L f_{\psi_4}}{\Delta x_1^2} + o\left(\Delta x_1^3\right) \quad (1.4a)$$

$$\alpha_i f_{\psi_{i-1}}^{"} + f_{\psi_i}^{"} + \beta_i f_{\psi_{i+1}}^{"} = r \frac{\left(f_{\psi_{i+1}} - 2 f_{\psi_i} + f_{\psi_{i-1}}\right)}{\Delta x_1^2} + o\left(\Delta x_1^4\right), \; i = 2.....\left(N_{x_1} - 2\right) \quad (1.4b)$$

$$f_{\psi_{N_{x_1}-1}}^{"} + \alpha_R f_{\psi_{N_{x_1}-2}}^{"} = \frac{a_R f_{N_{x_1}} + b_R f_{N_{x_1}-1} + c_R f_{N_{x_1}-2} + d_R f_{N_{x_1}-3} + e_R f_{N_{x_1}-4}}{\Delta x_1^2} + o\left(\Delta x_1^3\right) \quad (1.4c)$$

Equations (1.4a) - (1.4c) are solved simultaneously, using the known values of the function, **f** on the boundary nodes, at ψ_0 and $\psi_{N_{x_1}}$ and some guessed values on the non-boundary nodes, at ψ_i where, $i = 1.....\left(N_{x_1} - 1\right)$. The values of the coefficients involved in the equation (1.4) are the same as given, in the Table 1.1.

The matrix representation of the equation (1.4) is given by,

$$\left[A_{xx}\right] F_{xx} = \left[B_{xx}\right] f_R + f_{R_1} \quad (1.5)$$

where, A_{xx} and B_{xx} represent the matrices constructed from, collecting the values of the coefficients in the LHS and in the RHS of the system of equations (1.4a) - (1.4c),respectively. Similarly, F_{xx} and f_R represent the column vectors of the nodal (of non boundary) values in the LHS (of $\frac{\partial^2 f}{\partial x_1^2}$) and in the RHS (of function values) of the system of equations (1.4a) - (1.4c), respectively. The column vector f_{R_1} contains the constant values corresponding to the near boundary nodes, due to the Dirichlet boundary condition, which is imposed on the boundary nodes, on the two extreme points of the one-dimensional computational domain. The discrete values in the column vectors F_{xx}, f_R and f_{R_1} are sequenced, with respect to the indices of the nodes, belonging to the one-dimensional structured Cartesian uniform grid, about which the computations are performed.

Using equation (1.5), two formulae to compute the values of the partial derivative $\frac{\partial^2 f}{\partial x_1^2}$ at the n^{th} and $(n+1)^{th}$ time levels are deduced respectively as,

$$F_{xx}^n = \left[A_{xx}\right]^{-1}\left[B_{xx}\right] f_R^n + \left[A_{xx}\right]^{-1} f_{R_1}^n \quad (1.6)$$

$$F_{xx}^{n+1} = \left[A_{xx}\right]^{-1}\left[B_{xx}\right] f_R^{n+1} + \left[A_{xx}\right]^{-1} f_{R_1}^{n+1} \quad (1.7)$$

It should be noted that the above equations are for the non-boundary nodes, at ψ_i where, $i = 1.....\left(N_{x_1} - 1\right)$ located along the one-dimensional structured Cartesian uniform grid. The calculations in the equations (1.6) or (1.7) involve a tridiagonal matrix inversion, a matrix vector multiplication and one vector-vector addition.

IV. ALGORITHM TO SOLVE THE FULLY DISCRETIZED ONE-DIMENSIONAL DIFFUSION

STEP: 1

The compact scheme based interpolated values, of the partial derivative, $\frac{\partial^2 f}{\partial x_1^2}$ over the non-boundary nodes, at ψ_i where, $i = 1.....\left(N_{x_1} - 1\right)$ of the computational domain, at the n^{th} time level are computed, by solving the equation (1.6) over the one-dimensional grid line. In this computation, the value of the function, f on the boundary and the non-boundary nodes of the one-dimensional grid line are known, at the n^{th} time level (obtained from the initial condition).

STEP: 2

Thus after computing the values of the derivative term in the RHS of the equation (1.2a), as discussed in step 1 and with the values of the source term at the n^{th} and $(n+1)^{th}$ time levels are known a priori, the summation of terms in the RHS of the equation (1.2a) corresponding to each non-boundary node is computed. The resulting values are stored, in a column vector, c_R .

After storing the RHS value and function value in the equation (1.2a) corresponding to each non-boundary node, in the column vectors c_R and f_R, respectively its modified form is given by,

$$f_R^{n+1} - D_1 \frac{\Delta t}{2} \frac{\partial^2 f_R^{n+1}}{\partial x_1^2} = c_R^n \qquad (1.8)$$

The compact scheme based interpolated values, of the partial derivative, $\frac{\partial^2 f}{\partial x_1^2}$ over the non-boundary nodes, at ψ_i where, $i = 1.....\left(N_{x_1} - 1\right)$ of the computational domain, at the $(n+1)^{th}$ time level are computed, by solving the equation (1.7) over the one dimensional grid line. In this computation, the value of the function, f on the boundary nodes at the $(n+1)^{th}$ time level are known from the given boundary conditions. For the non-boundary nodes at the $(n+1)^{th}$ time level some guessed values are used.

Approximating, the spatial derivatives, $\frac{\partial^2 f}{\partial x_1^2}$ at the $(n+1)^{th}$ time level, using the equation (1.7), the fully discretized form of the equation (1.8) is given by,

$$f_R^{n+1} - D_1 \frac{\Delta t}{2} [A_{xx}]^{-1} [B_{xx}] f_R^{n+1} = c_R^n + D_1 \frac{\Delta t}{2} [A_{xx}]^{-1} f_{R_1}^{n+1} \qquad (1.9)$$

Factorizing, $[A_{xx}]^{-1}$ in the LHS of the equation (1.9) leads to,

$$[A_{xx}]^{-1} \left([A_{xx}] - D_1 \frac{\Delta t}{2} [B_{xx}] \right) f_R^{n+1} = c_R^n + D_1 \frac{\Delta t}{2} [A_{xx}]^{-1} f_{R_1}^{n+1} \qquad (1.10)$$

Equating the matrix $\left([A_{xx}] - D_1 \frac{\Delta t}{2} [B_{xx}] \right)$, to a matrix, $[T_{xx}]$, the equation (1.10) reduces to,

$$[A_{xx}]^{-1} [T_{xx}] f_R^{n+1} = c_R^n + D_1 \frac{\Delta t}{2} [A_{xx}]^{-1} f_{R_1}^{n+1} \qquad (1.11)$$

Pre-multiplying, the equation (1.11) with the matrix, $[A_{xx}]$ leads to,

$$[T_{xx}] f_R^{n+1} = [A_{xx}] c_R^n + D_1 \frac{\Delta t}{2} f_{R_1}^{n+1} \qquad (1.12)$$

Finally, equation (1.12) is solved over the one-dimensional grid line, to obtain the value of the function, f at the $(n+1)^{th}$ time level on the non-boundary nodes of the computational domain. The calculations in the RHS of the equation (1.12) involve, a matrix vector multiplication and a vector-vector addition. Whereas, in its LHS, the coefficient matrix, $[T_{xx}]$ has a pentadiagonal structure. The matrix equations (1.12) is solved iteratively, using the Bi-CGSTAB(2) algorithm, as referred in Saad, 1996. This iteration procedure is continued, until the set convergence for the true error norm of the numerical solution, corresponding to the $(n+1)^{th}$ time level is attained. The solution is marched in time, by solving the equation (1.2a) recursively, for the succeeding time steps, by following the steps 1 and 2, of the algorithm discussed so far.

V. COMPACT SCHEMES FOR THE SPATIAL DISCRETIZATION OF THE TWO DIMENSIONAL DIFFUSION EQUATION

Using the D'yakanov splitting technique (Thomas, 1998), the equation (1.3) is given by,

$$\left(1 - D_1 \frac{\Delta t}{2} \frac{\partial^2}{\partial x_1^2}\right) \tilde{f}_{i,j}^{n+1} = \left(1 + D_1 \frac{\Delta t}{2} \frac{\partial^2}{\partial x_1^2}\right) \tilde{f}_{i,j}^{n} + \frac{\Delta t}{2} \left[g\left(x_{1i}, x_{2j}, t\right)^{n+1} + g\left(x_{1i}, x_{2j}, t\right)^{n} \right] \qquad (1.13)$$

where,

$$\left(1 - D_2 \frac{\Delta t}{2} \frac{\partial^2}{\partial x_2^2}\right) f_{i,j}^{n+1} = \tilde{f}_{i,j}^{n+1} \qquad (1.14)$$

and

$$\left(1 + D_2 \frac{\Delta t}{2} \frac{\partial^2}{\partial x_2^2}\right) f_{i,j}^{n} = \tilde{f}_{i,j}^{n} \qquad (1.15)$$

The partial derivative, $\frac{\partial^2 f}{\partial x_2^2}$ only on the non-boundary nodes, at ψ_j where, $j = 1.....\left(N_{x_2} - 1\right)$ located along a particular vertical grid line of a two-dimensional structured Cartesian uniform grid are approximated, using the system of compact schemes.

A system of compact schemes used, to approximate the second order partial derivative, only on the non-boundary nodes located along a particular vertical grid line of a two-dimensional structured Cartesian uniform using the known values of the function, f on the boundary nodes, at ψ_0 and $\psi_{N_{x2}}$ and some guessed values on the non-boundary nodes, at ψ_j where, $j = 1.....\left(N_{x_2} - 1\right)$ are given in the Table 1.2 which are calculated on vertical grid.

Using the two formulae to compute the values of the partial derivative, $\frac{\partial^2 f}{\partial x_2^2}$ at the n^{th} and $\left(n+1\right)^{th}$ time levels are deduced respectively as,

$$F_{yy}^{n} = \left[A_{yy}\right]^{-1}\left[B_{yy}\right] f_C^{n} + \left[A_{yy}\right]^{-1} f_{C_1}^{n} \qquad (1.16)$$

$$F_{yy}^{n+1} = \left[A_{yy}\right]^{-1}\left[B_{yy}\right] f_C^{n+1} + \left[A_{yy}\right]^{-1} f_{C_1}^{n+1} \qquad (1.17)$$

It should be noted that the above equations are for the non-boundary nodes, at ψ_j where, $j = 1.....\left(N_{x_2} - 1\right)$ located along a particular vertical grid line of a two dimensional structured Cartesian uniform grid. The calculations in the equations (1.16) or (1.17) involve a tridiagonal matrix inversion, a matrix vector multiplication and one vector-vector addition.

A system of compact schemes used, to approximate the values of the partial derivative, $\frac{\partial^2 \tilde{f}}{\partial x_2^2}$ only on the non-boundary nodes, at ψ_i where, $i = 1.....\left(N_{x_1} - 1\right)$ located along a particular horizontal grid line (shown in Figure 1) of a two-dimensional structured Cartesian uniform grid are given by,

$$\tilde{f}''_{\psi_1} + \alpha_L \tilde{f}''_{\psi_2} = \frac{a_L \tilde{f}_{\psi_0} + b_L \tilde{f}_{\psi_1} + c_L \tilde{f}_{\psi_2} + d_L \tilde{f}_{\psi_3} + e_L \tilde{f}_{\psi_4}}{\Delta x_1^2} + o\left(\Delta x_1^3\right)$$

(1.18a)

$$\alpha_i \tilde{f}''_{\psi_{i-1}} + \tilde{f}''_{\psi_i} + \beta_i \tilde{f}''_{\psi_{i+1}} = r\frac{\left(\tilde{f}_{\psi_{i+1}} - 2\tilde{f}_{\psi_i} + \tilde{f}_{\psi_{i-1}}\right)}{\Delta x_1^2} + o\left(\Delta x_1^4\right), \quad i = 2.....\left(N_{x_1} - 2\right)$$

(1.18b)

$$\tilde{f}''_{\psi_{N_{x_1}-1}} + \alpha_R \tilde{f}''_{\psi_{N_{x_1}-2}} = \frac{a_R \tilde{f}_{N_{x_1}} + b_R \tilde{f}_{N_{x_1}-1} + c_R \tilde{f}_{N_{x_1}-2} + d_R \tilde{f}_{N_{x_1}-3} + e_R \tilde{f}_{N_{x_1}-4}}{\Delta x_1^2} + o\left(\Delta x_1^3\right)$$

(1.18c)

Equations (1.18a) - (1.18c) are solved simultaneously, using the known values of the function, $\tilde{f}$ on the boundary nodes, at ψ_0 and $\psi_{N_{x_1}}$ and some guessed values on the non-boundary nodes, at ψ_i where, $i = 1.....\left(N_{x_1} - 1\right)$. The values of the coefficients involved in the equations (1.18) are determined using two-dimensional structured Cartesian uniform grid are given in Table 1.2. In analogy with the matrix representation of the equation (1.18) is given by,

$$\left[A_{xx}\right] F_{xx} = \left[B_{xx}\right] \tilde{f}_R + \tilde{f}_{R_1} \qquad (1.19)$$

where, A_{xx} and B_{xx} represent the matrices constructed from the values of the coefficients in the LHS and in the RHS of the system of equations (1.18a) - (1.18c), respectively. Similarly, F_{xx} and $\tilde{f}_R$ represent the column vectors of the nodal (of non boundary) values in the LHS (of $\frac{\partial^2 \tilde{f}}{\partial x_1^2}$) and in the RHS (of function values) of the system of equations (1.18a) - (1.18c), respectively. The column vector $\tilde{f}_{R_1}$ contains the constant values corresponding to the near boundary nodes, due to the Dirichlet boundary condition, which is imposed on the nodes along the left and right boundaries of the two dimensional computational domain. The discrete values in the column vectors F_{xx}, $\tilde{f}_R$ and $\tilde{f}_{R_1}$ are sequenced, with respect to the indices of the nodes, belonging to a particular horizontal grid line, about which the computations are performed.

Using the equation (1.19), two formulae to compute the values of the partial derivative, $\frac{\partial^2 \tilde{f}}{\partial x_1^2}$ at the n^{th} and $\left(n+1\right)^{th}$ time levels are deduced respectively as,

$$F_{xx}^{n} = \left[A_{xx}\right]^{-1}\left[B_{xx}\right] \tilde{f}_R^{n} + \left[A_{xx}\right]^{-1} \tilde{f}_{R_1}^{n} \qquad (1.20)$$

$$F_{xx}^{n+1} = \left[A_{xx}\right]^{-1}\left[B_{xx}\right] \tilde{f}_R^{n+1} + \left[A_{xx}\right]^{-1} \tilde{f}_{R_1}^{n+1} \qquad (1.21)$$

It should be noted that the above equations are for the non-boundary nodes, at ψ_i where, $i = 1.....\left(N_{x_1} - 1\right)$ located along a particular horizontal grid line of a two dimensional structured Cartesian uniform grid. The calculations in the equations (1.20)or (1.21) involve a tridiagonal matrix inversion, a matrix vector multiplication and one vector-vector addition.

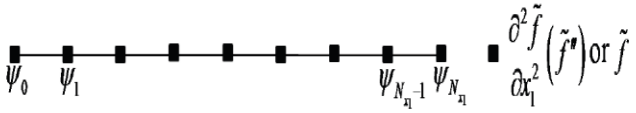

Figure 1: One-dimensional structured Cartesian uniform grid used to approximate the partial derivative $\frac{\partial^2 f}{\partial x_1^2}$ on a non-periodic Computational Domain

Table 1.1: Values of the coefficients in the equations (1.4a) - (1.4c)

Left near boundary node	Interior node	Right near boundary node
$\alpha_L = -1.0$	$\alpha = \frac{1.0}{10.0}$	$\alpha_R = \alpha_L$
$a_L = 1.0$	$\beta = \frac{1.0}{10.0}$	$a_R = a_L$
$b_L = -3.0$	$\gamma = \frac{12.0}{10.0}$	$b_R = b_L$
$c_L = 3.0$	---	$c_R = c_L$
$d_L = 1.0$	---	$d_R = d_L$

Table 1.2 : Values of the coefficients in the vertical grid for equations (1.4a) - (1.4c)

Left near boundary node	Interior node	Right near boundary node
$\alpha_L = 11.0$	$\alpha = \frac{1.0}{10.0}$	$\alpha_R = \alpha_L$
$a_L = 13.0$	$\beta = \frac{1.0}{10.0}$	$a_R = a_L$
$b_L = -27.0$	$\gamma = \frac{12.0}{10.0}$	$b_R = b_L$
$c_L = 15.0$	---	$c_R = c_L$
$d_L = -1.0$	---	$d_R = d_L$

VI. ALGORITHM TO SOLVE THE FULLY DISCRETIZED TWO-DIMENSIONAL DIFFUSION EQUATIONS

STEP:1

The fully discretized form of the equation (1.15) (for the non-boundary nodes located on a vertical grid line), after substituting the equation (1.16) is given by,

$$f_C^n + D_2 \frac{\Delta t}{2}\left(\left[A_{yy}\right]^{-1}\left[B_{yy}\right] f_C^n + \left[A_{yy}\right]^{-1} f_{C_1}^n\right) = \tilde{f}_C^n \quad (1.22)$$

Factorizing, $\left[A_{yy}\right]^{-1}$ from the first two terms in the LHS of the equation (1.22) leads to,

$$\left[A_{yy}\right]^{-1}\left(\left[A_{yy}\right] + D_2 \frac{\Delta t}{2}\left[B_{yy}\right]\right) f_C^n + D_2 \frac{\Delta t}{2}\left[A_{yy}\right]^{-1} f_{C_1}^n = \tilde{f}_C^n \quad (1.23)$$

Equating, the matrix, $\left(\left[A_{yy}\right] + D_2 \frac{\Delta t}{2}\left[B_{yy}\right]\right)$ to a matrix, $\left[T_{yy}^{'}\right]$, the equation (1.23) reduces to,

$$\left[A_{yy}\right]^{-1}\left[T_{yy}^{'}\right] f_C^n + D_2 \frac{\Delta t}{2}\left[A_{yy}\right]^{-1} f_{C_1}^n = \tilde{f}_C^n \quad (1.24)$$

Pre-multiplying, the equation (1.24) with the matrix, $\left[A_{yy}\right]$ and after further rearrangement leads to,

$$\left[A_{yy}\right]\tilde{f}_C^n = \left[T_{yy}^{'}\right] f_C^n + D_2 \frac{\Delta t}{2} f_{C_1}^n \quad (1.25)$$

where the matrix, $\left[A_{yy}\right]$ has the tridiagonal matrix structure.

Equation (1.25) is solved over each of the vertical grid lines $\left(i = 0.....N_{x_1}\right)$. In this computation, the f values on the nodes of the horizontal grid lines $\left(j = 0 \text{ and } j = N_{x_2}\right)$ as well as on the entire non-boundary nodes, corresponding to the nth time level are known a priori.

Thus, the compact scheme based interpolated values of the function, $\tilde{f}$ at the n^{th} time level, over the entire boundary and the non-boundary nodes of the computational domain are computed. The calculations in the RHS of the equation (1.25) involve a matrix vector multiplication and a vector-vector addition. In its LHS, the coefficient matrix, $\left[A_{yy}\right]$ has a tridiagonal structure. The matrix equation (1.25) is solved directly by inverting the matrix, $\left[A_{yy}\right]$ using the standard TDMA algorithm.

STEP:2

The fully discretized form of the first term in the RHS of the equation (1.13) (for the non-boundary nodes located on a horizontal grid line), after substituting the equation (1.20) is given by,

$$\tilde{f}_R^n + D_1 \frac{\Delta t}{2}\left(\left[A_{xx}\right]^{-1}\left[B_{xx}\right]\tilde{f}_R^n + \left[A_{xx}\right]^{-1} f_{R_1}^n\right)$$

Factorizing, $\left[A_{xx}\right]^{-1}$ gives

$$\left[A_{xx}\right]^{-1}\left(\left[A_{xx}\right] + D_1 \frac{\Delta t}{2}\left[B_{xx}\right]\right)\tilde{f}_R^n + + D_1 \frac{\Delta t}{2}\left[A_{xx}\right]^{-1} f_{R_1}^n$$

Equating, the matrix, $\left(\left[A_{xx}\right] + D_1 \frac{\Delta t}{2}\left[B_{xx}\right]\right)$ to a matrix, $\left[T_{xx}^{'}\right]$ the above written expression reduces to,

$$\left[A_{xx}\right]^{-1}\left[T_{xx}^{'}\right]\tilde{f}_R^n + + D_1 \frac{\Delta t}{2}\left[A_{xx}\right]^{-1} f_{R_1}^n$$

The matrix-vector computations in the above written expression is carried out on each of the horizontal grid lines $\left(j = 1.....\left(N_{x_2} - 1\right)\right)$. In this computation, the $\tilde{f}$ values on the nodes of the vertical grid lines $\left(i = 0 \text{ and } i = N_{x_1}\right)$ as well as on the entire non-boundary nodes, corresponding to the n^{th} time level are known a priori. Thus, the compact scheme based interpolated values of

the term $\left(1+D_1\frac{\Delta t}{2}\frac{\partial^2}{\partial x_1^2}\right)\tilde{f}_{i,j}^{\,n}$ in the RHS of the equation (1.13) are computed, over the entire non-boundary nodes of the computational domain.

Having computed the values of the term $\left(1+D_1\frac{\Delta t}{2}\frac{\partial^2}{\partial x_1^2}\right)\tilde{f}_{i,j}^{\,n}$ at the n^{th} time level and the values of the source term at the n^{th} and $(n+1)^{th}$ time level are known a priori, the summation of the terms in the RHS of the equation (1.13) corresponding to each non-boundary node is computed and stored in a array, $c_{i,j}$.

After storing the value of the RHS of the equation (1.13) corresponding to each non-boundary node, in the array $c_{i,j}$, its modified form is given by,

$$\left(1+D_1\frac{\Delta t}{2}\frac{\partial^2}{\partial x_1^2}\right)\tilde{f}_{i,j}^{\,n}=c_{i,j} \quad (1.26)$$

STEP:3

The fully discretized form of the equation (1.14) (for the non-boundary nodes located on a vertical grid line), after substituting the equation (1.17) is given by,

$$f_C^{n+1}-D_2\frac{\Delta t}{2}\left(\left[A_{yy}\right]^{-1}\left[B_{yy}\right]f_C^{n+1}+\left[A_{yy}\right]^{-1}f_{C_1}^{n+1}\right)=\tilde{f}_C^{n+1} \quad (1.27)$$

Factorizing, $\left[A_{yy}\right]^{-1}$ from the first two terms in the LHS of the equation (1.27) leads to,

$$\left[A_{yy}\right]^{-1}\left(\left[A_{yy}\right]-D_2\frac{\Delta t}{2}\left[B_{yy}\right]\right)f_C^{n+1}-D_2\frac{\Delta t}{2}\left[A_{yy}\right]^{-1}f_{C_1}^{n+1}=\tilde{f}_C^{n+1} \quad (1.28)$$

Equating, the matrix, $\left(\left[A_{yy}\right]-D_2\frac{\Delta t}{2}\left[B_{yy}\right]\right)$ to a matrix, $\left[T_{yy}\right]$, the equation (1.28) reduces to,

$$\left[A_{yy}\right]^{-1}\left[T_{yy}\right]f_C^{n+1}-D_2\frac{\Delta t}{2}\left[A_{yy}\right]^{-1}f_{C_1}^{n+1}=\tilde{f}_C^{n+1} \quad (1.29)$$

Pre-multiplying, the equation (1.29) with the matrix, $\left[A_{yy}\right]$ and with further rearrangement leads to,

$$\left[A_{yy}\right]\tilde{f}_C^{n+1}=\left[T_{yy}\right]f_C^{n+1}-D_2\frac{\Delta t}{2}f_{C_1}^{n+1} \quad (1.30)$$

Equation (1.30) is solved over the vertical grid lines, $i=0$ and $i=N_{x_1}$ (bounding the left and right boundaries). In this computation, the $\tilde{f}$ values at the $(n+1)^{th}$ time level are already known on the boundaries of the two-dimensional computational domain (obtained from the boundary conditions).

Thus, the compact scheme based interpolated values of the function, f at the $(n+1)^{th}$ time level over the near-boundary and the interior nodes of the left and right boundaries of the two-dimensional computational domain are computed. The calculations in the RHS of the equation (1.30) involve a matrix vector multiplication and a vector subtraction. In the LHS, the coefficient matrix, $\left[A_{yy}\right]$ has a tridiagonal structure. The matrix equation (1.30) is solved directly, by inverting the matrix, $\left[A_{yy}\right]$ using the standard TDMA algorithm.

STEP:4

The fully discretized form of the equation (1.26) (for the non-boundary nodes located on a horizontal grid line), after substituting the equation (1.21) is given by,

$$\tilde{f}_R^{n+1}-D_1\frac{\Delta t}{2}\left(\left[A_{xx}\right]^{-1}\left[B_{xx}\right]\tilde{f}_R^{n+1}+\left[A_{xx}\right]^{-1}f_{R_1}^{n+1}\right)=c_R^n \quad (1.31)$$

The values of the column vector, c_R^n in the equation (1.31) is obtained from the array, $c_{i,j}$, for a particular horizontal grid line.

Factorizing, $\left[A_{xx}\right]^{-1}$ from the first two terms in the LHS of the equation (1.31) leads to,

$$\left[A_{xx}\right]^{-1}\left(\left[A_{xx}\right]-D_1\frac{\Delta t}{2}\left[B_{xx}\right]\right)\tilde{f}_R^{n+1}-D_1\frac{\Delta t}{2}\left[A_{xx}\right]^{-1}f_{R_1}^{n+1}=c_R^n \quad (1.32)$$

Equating, the matrix, $\left(\left[A_{xx}\right]-D_1\frac{\Delta t}{2}\left[B_{xx}\right]\right)$ to a matrix, $\left[T_{xx}\right]$, the equation (1.32) reduces to,

$$\left[A_{xx}\right]^{-1}\left[T_{xx}\right]\tilde{f}_R^{n+1}-D_1\frac{\Delta t}{2}\left[A_{xx}\right]^{-1}f_{R_1}^{n+1}=c_R^n \quad (1.33)$$

Pre-multiplying, the equation (1.33) with the matrix, $\left[A_{xx}\right]$ and with further rearrangement leads to,

$$\left[T_{xx}\right]\tilde{f}_R^{n+1}=\left[A_{xx}\right]c_R^n+D_1\frac{\Delta t}{2}f_{R_1}^{n+1} \quad (1.34)$$

Equation (1.34) is solved over each of the horizontal grid lines indexed between $\left(j=1.....\left(N_{x_2}-1\right)\right)$. Thus, the compact scheme based interpolated values of the function, $\tilde{f}$ at the $(n+1)^{th}$ time level, over the entire non-boundary nodes of the computational domain are computed.

STEP:5

Finally, by rearranging the equation (1.30), the formula to compute the values of the function, f at the $(n+1)^{th}$ time level, over the non-boundary nodes located along each of the vertical grid lines $\left(i=1.....\left(N_{x_1}-1\right)\right)$. of the two-dimensional structured Cartesian uniform grid is deduced to be,

$$\left[T_{yy}\right]f_C^{n+1}=\left[A_{yy}\right]\tilde{f}_C^{n+1}+D_2\frac{\Delta t}{2}f_{C_1}^{n+1} \quad (1.35)$$

In this computation, the values of the function, $\tilde{f}$ at the $(n+1)^{th}$ time level, over the entire non-boundary nodes of the computational domain are known a priori, from the step 4. Similarly, the values the function, f at the $(n+1)^{th}$ time level, over the nodes located along the horizontal grid lines indexed $j=0$ and $j=N_{x_2}$, respectively (representing for the bottom and top boundaries) are known a priori, from the boundary condition.

Thus, the compact scheme based interpolated values of the function, f at the $(n+1)^{th}$ time level, over the entire non-boundary nodes, of the two-dimensional computational domain are computed. The calculations in the RHS of the equations (1.34) or (1.35) involve, a matrix vector multiplication and a vector-vector addition. In the LHS, the coefficient matrix, T_{xx} or T_{yy} has a pentadiagonal structure. The matrix equations(1.34) or (1.35) are solved iteratively using the Bi-CGSTAB(2) algorithm as refered in Saad, 1996. This iteration procedure is continued, until the set convergence for the true error norm of the numerical solution, corresponding to the $(n+1)^{th}$ time level is attained. The solution is marched in time, by solving the equation (1.3) recursively, for the succeeding time steps, following the steps 1 to 5, of the algorithm discussed so far.

VII. TEST PROBLEMS

In this section, the higher order spatial accuracy of the developed, central difference based compact schemes for the one and two-dimensional diffusion equations are validated, by solving numerically two test problems. The exact solutions of these problems satisfy the respective governing PDE, subjected to an initial condition and Dirichlet boundary conditions. In the case of numerical scheme developed for the LPPDE, the iterative matrix include the terms due to the discretization of the time derivative and the second order spatial derivative(s).

PROBLEM: 1

$$f(x_1,t)=\exp\left(-2\pi^2 t\right)\sin(\pi x_1),\ 0\le x_1\le 1, 0\le t\le 1.0 \quad (1.36a)$$

$$g(x_1,t)=\pi\exp\left(-2\pi^2 t\right)\left[\left(D_1-2.0\right)\pi\sin(\pi x_1)\right] \quad (1.36b)$$

Equation (1.36) represents the exact solution along with the source term which satisfies the one-dimensional diffusion equation restricted over a domain, $0\le x_1\le 1$. The value of the diffusion coefficient D_1 is assumed to be 1.0. The Dirichlet boundary and initial conditions for this problem are derived from the given exact solution. A schematic of the computational domain along with the initial and boundary conditions is shown, in the Figure 2.

The grid sizes chosen to conduct numerical experiments on this one-dimensional problem include 11, 17, 21, 26, 33, 41, 51, 65, 81, 101, 129, 161, 201 and 257 The simulation is run until the solution evolves for the total time of 1.0 unit. In order to determine the optimum time step, the fully discretized equations based on compact 4^{th} order and conventional 2^{nd} order schemes are solved, respectively on the finest grid (257).The time step values chosen for the numerical experiment ranges between $5\text{x}10^{-7}$ to10^{-3}.

VIII. RESULTS

From the log-log plot of the l_2 true error norm, as a function of number of time steps (N_t) shown, in the Figure 3(a), it is clear that, the time step value chosen for the calculation has a considerable influence on the solution accuracy. It shows that, for the compact scheme based solutions, until the time step of $5\text{x}10^{-4}$, the l_2 true error norm obtained, at the end of simulation is of order 10^{-4}. But with further reduction in the time step, starting from 10^{-4} until $5\text{x}10^{-7}$, the error norm has drastically reduced to the order of 10^{-12}.

Specifically, up to the time step of $5\text{x}10^{-6}$ the reduction is monotonic. There after, the l_2 true error norm value is just fluctuated about 10^{-12}. Similarly, for the conventional 2^{nd} order scheme based solutions, until the time step of $5\text{x}10^{-4}$, l_2 true error norm behavior is similar to the compact scheme based solution. Exactly, at the time step of 10^{-4}, the true error norm of the conventional 2^{nd} order scheme based solutions, obtained at the end of simulation is in the order of 10^{-10}. Thereafter, with reduction in the time step, there is no further reduction in the true error norm and remain constant. Based on the trend followed in the Figure 3(a), for both compact and conventional spatial schemes based solutions, a reasonable time step of 10^{-6} is elected and used for the grid independence study.

From the log-log plot of the l_2 true error norm, as a function of number of nodes (N) shown, in the Figure 3(b), it is noticed that, the compact scheme fetches higher order accurate solution than that based on the conventional scheme. In addition, the log-log plots of the l_2 norm of the true error, as a function of number of nodes (N) shown, in the Figure 3(c) clearly illustrate the higher order of accuracy of numerical solution produced using the compact scheme.

Similarly, from the log-log plot of the iterative history of the l_2 true error norm shown, in Figure 3(d), it is clear that, on all the grids chosen for analysis, the solutions obtained using the compact 4^{th} order and conventional 2^{nd} order schemes have satisfied the convergence theorem. Further, there is some significant difference in the trends of the true error norm history arrived using 2^{nd} order and 4^{th} order schemes, as a function of grid density.

Specially, for the solution produced using conventional 2^{nd} order scheme, among several grids, the increase in the rate of convergence of the solution, between any two consecutive coarse and finer grids is gradual and uniform. Whereas, in the case of the solution produced using compact 4^{th} order scheme, among several grids, the increase in the rate of convergence of the solution, between any two consecutive coarse and finer grids is not uniform. It increases with increase in the relative grid density between the two successive grids.

For this particular problem, the rate of convergence of the solution based on the 4^{th} order compact scheme is found, to be less oscillatory, when compared that based on the 2^{nd} order scheme. Therefore, for the set number of iterations based on the time step, compact 4^{th} order scheme is able to achieve the maximum possible reduction in the l_2 norm of the true error, when compared to that achieved, using the conventional 2^{nd} order scheme. Further, within the set number of iterations, due to the less oscillatory nature of the compact 4^{th} order scheme based iterative matrix, in addition to the faster attenuation of high frequency error components, some of the low frequency error components are also be attenuated. This leads to the increase in the rate of convergence and accuracy of the numerical solution produced, using the 4^{th} order compact scheme. From this test problem, it can be clear that, though the range of high frequency error components increases with increase in fineness of the grid, the intensity of the oscillatory nature in the error propagation is dependent, on the inherent smoothness of the function, which satisfies the model equation and the optimum time step value.

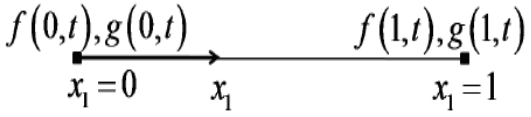

Figure 2: A schematic of the computational domain along with initial and boundary conditions, used to solve the one-dimensional diffusion equation

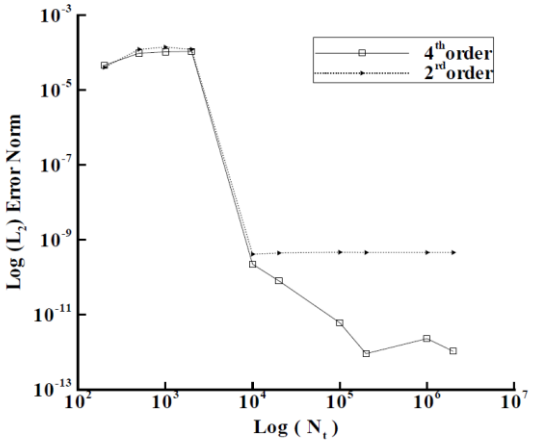

Figure 3: (a) Determination of optimum time step from the fine grid solutions.

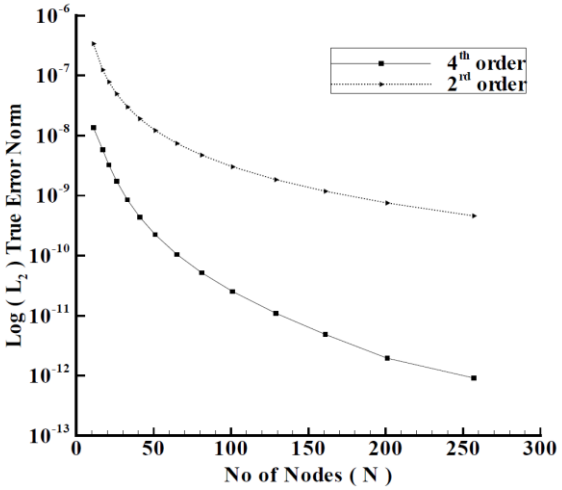

Figure 3: (b) Comparison of grid refinement study of order of accuracy between compact 4^{th} order and conventional 2^{nd} order schemes.

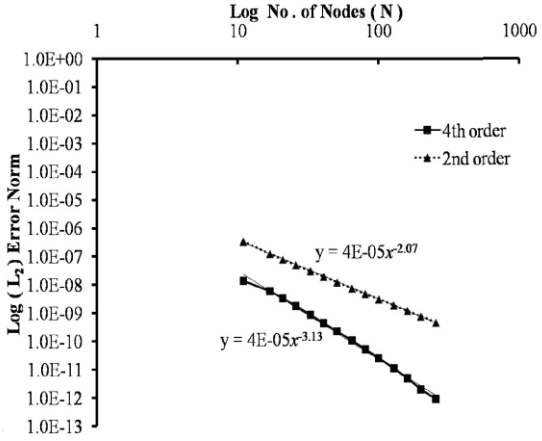

Figure 3: (c) Log-Log plot of comparison of grid refinement study of order of accuracy between compact 4^{th} order and conventional 2^{nd} order schemes.

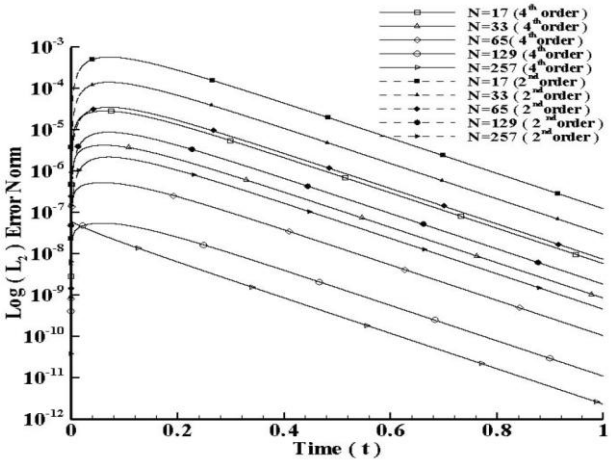

Figure 3: (d) Comparison of rate of convergence of solution between compact 4^{th} order and conventional 2^{nd} order schemes.

PROBLEM: 2

$$f(x_1,x_2,t)=e(-\pi^2 t)\sin(\pi x_1)\sin(\pi x_2), 0\le x_1\le 1, 0\le x_2\le 1, 0\le t\le 1.0 \quad (1.37a)$$

$$g(x_1,x_2,t)=\pi^2 e(-\pi^2 t)\sin(\pi x_1)\sin(\pi x_2)[D_1+D_2-1] \quad (1.37b)$$

The equation (1.37) represents the exact solution along with the source term which satisfiesthe two-dimensional diffusion equation restricted over a square domain $0\le x_1\le 1$ and $0\le x_2\le 1$. The values of D_1 and D_2 are assumed to be 1.0. The Dirichlet boundary and initial conditions are derived from the given exact equation. A schematic of the computational domain along with the initial and boundary conditions is shown, in the Figure 4.

The grid sizes chosen to conduct the numerical experiments on this two-dimensional problem include,
11x11,17x17, 21x21, 26x26, 33x33, 41x41, 51x51, 65x65, 81x81, 101x101,129x129, 161x161, 201x201and 257x257.

The simulations run until the solution evolves for the total time of 1.0 unit. In order to determine the optimum time step, the fully discretized equations based on compact 4^{th} order and conventional 2^{nd} order schemes are solved, respectively on the finest grid $(257x257)$. The time step values chosen for the numerical experiment ranges between 10^{-6} to 10^{-3}.

RESULTS

From the log-log plot of the l_2 true error norm, as a function of number of time steps (N_t) shown, in the Figure 5(a), it is clear that, the time step value chosen for the calculation influence considerably the solution accuracy. It shows that, for the both compact 4^{th} and conventional 2^{nd} order schemes based solutions, between the time steps of $5x10^{-3}$ until 10^{-3}, the true l_2 error norm obtained, at the end of simulation lies in the range of 10^{-5}. With the reduction in the time step, exactly at $1x10^{-4}$,the error norm reduces to the order of 10^{-9}, for the both schemes. Thereafter, with further reduction in the time step, the difference in the l_2 true error norm for the 2^{nd} order scheme, becomes independent of variation in the time step and is maintained in the range of 10^{-9}. Whereas, in the case of compact schemes the error norm reduction is considerable and it becomes stable at 10^{-12}. Based on the trend followed in the Figure5(a), for both compact and conventional spatial schemes based solutions, a reasonable time step of $5x10^{-6}$ is selected and used for the grid independence study.

From the log-log plot of the l_2 true error norm as a function of number of nodes(N)shown, in the Figure 5(b), it is noticed that, on the finest grid size of $257x257$ the compact scheme is able to attain the error norm value in the order of 10^{-13}. Whereas, on the same grid size, the 2^{nd} order scheme fetches only the error norm reduction in the order of 10^{-9}. This result proves the feasibility in attaining higher order accuracy of the compact scheme for a multi-dimensional problem. In addition, the log-log plots of the l_2 norm of the true error, as a function of number of nodes (N) shown, in the Figure5(c) clearly illustrate the higher order of accuracy of numerical solution produced using the compact scheme.

Similarly, from the log-log plot of the iterative history of the l_2 norm of the true error shown, in Figure 5(d), it is clear that, on all the grids chosen for the analysis, the solutions obtained using the compact 4^{th} order and conventional 2^{nd} order schemes have satisfied the convergence theorem.

Further, the iterative l_2 true error norm history depicts, the superior rate of convergence attainable by the compact scheme on both the coarser and finer grids, when compared with the same based on the conventional 2^{nd} order scheme.

For this particular problem, the rate of convergence of the solution based on the 4^{th} order compact scheme is found to be better, when compared that based on the 2^{nd} order scheme. Therefore, for the chosen number of iterations based on the time step, compact 4^{th} order scheme is able to achieve the maximum possible reduction in the l_2 norm of the true error when compared to that achieved using the conventional 2^{nd} order scheme. Further, within the chosen number of iterations, due to the less oscillatory nature of the iterative matrix, based on the compact 4^{th} order scheme, in addition to the faster attenuation of high frequency error components, some of the low frequency error components could also be attenuated. This leads to the increase in the rate of convergence and accuracy of the numerical solution.

From this test problem, it is clear that, though the range of high frequency error components increase with the increase in fineness of the grid, the intensity of oscillatory nature in the error propagation is dependent, on the inherent smoothness of the function, which satisfies the model equation and the optimum time step value.

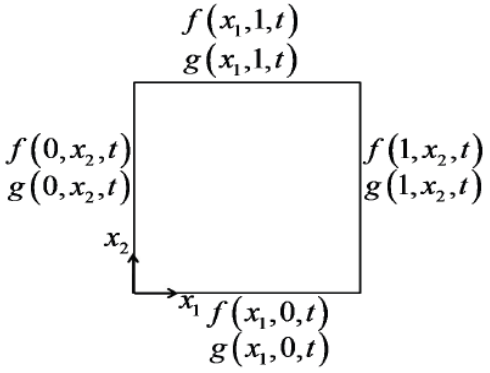

Figure 4: A schematic of the computational domain along with initial and boundary conditions used to solve the in two-dimensional Diffusion equation

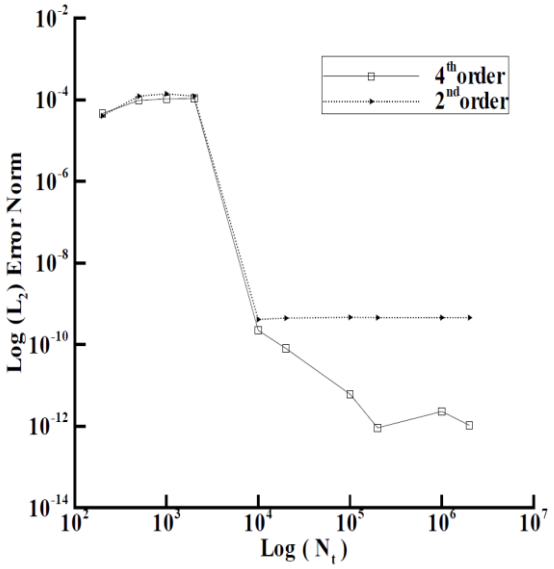

Figure 5: (a) Determination of optimum time step from the fine grid solutions.

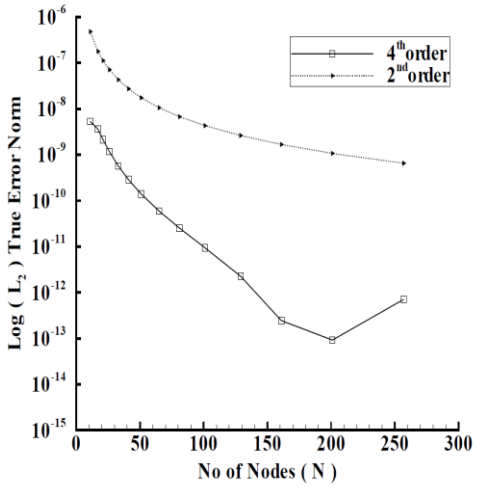

Figure 5: (b) Comparison of grid refinement study of order of accuracy between compact 4^{th} order and conventional 2^{nd} order schemes.

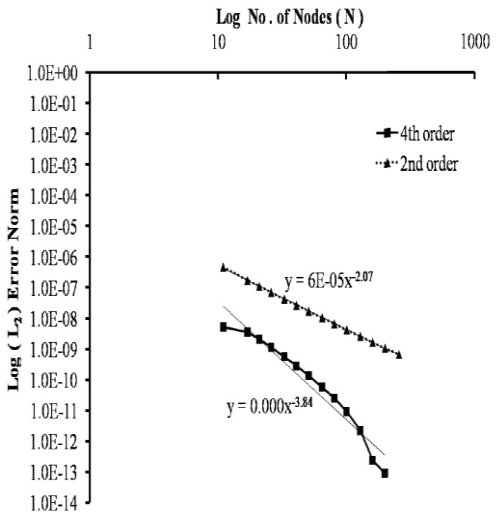

Figure 5: (c) Log-Log plot of comparison of grid refinement study of order of accuracy between compact 4^{th} order and conventional 2^{nd} order schemes.

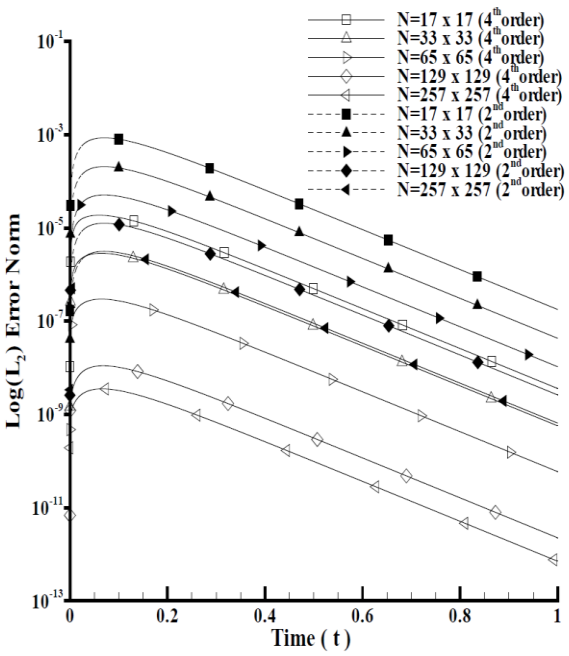

Figure 5: (d) Comparison of rate of convergence of solution between compact 4^{th} order and conventional 2^{nd} order schemes.

IX. CONCLUSION

The construction of the numerical scheme involves a factorization procedure, which will contribute to the splitting errors. Therefore, it is imperative to compare and understand the influence of the time step and the splitting error due to factorization, on the stability of the iterative matrices constructed, using the compact 4^{th} order and the conventional 2^{nd} order schemes.

The interest is to demonstrate the higher order spatial accuracy and the better rate of convergence of the solution produced using the developed compact 4^{th} order scheme, when compared with the same produced, using the conventional 2^{nd} order scheme. The assessment is made, in terms of the discrete l_2 or l_∞ norm of the true error of the converged numerical solution. This particular estimate is made, using the true error data corresponding to the non-boundary nodes of the computational domain.

From the two dimensional problem, it is clear that, though the range of high frequency error components increase with the increase in fineness of the grid, the intensity of oscillatory nature in the error propagation is dependent, on the inherent smoothness of the function, which satisfies the model equation and the optimum time step value.

REFERENCES

1. Jost, J. (2002), Partial Differential Equations, New York: Springer-Verlag.
2. Thomas, Numerical Partial Differential Equations: Finite Difference Methods. Springer-Verlag, New york, 1998.

3. El-Mikkawy, M. E. A. (2005). A new computational algorithm for solving periodic tri-diagonal linear systems. Applied Mathematics and Computations, 161, 691–696.
4. Ciment, M., S. H. Leventhal, and B. C. Weinberg (1978). The operator compact implicit method for parabolic equations. Journal of Computational Physics, 28, 135–166.
5. Adam, Y. (1977). Highly accurate compact implicit methods and boundary conditions.Journal of Computational Physics, 24, 10–22.
6. Kampanis, N. A. and J. A. Ekaterinaris (2006). A staggered grid, high-order accurate method for the incompressible Navier-Stokes equations. Journal of Computational Physics, 215, 589–613.
7. You, D. (2006). A high-order Padé ADI method for unsteady convection-diffusion equations. Journal of Computational Physics, 214, 1–11.
8. Chang, H.-R. and H. N. Shirer (1985). Compact spatial differencing techniques in numerical modeling. Monthly Weather Review, 113, 409–423.
9. Abide, S. and S. Viazzo (2005). A 2D compact fourth-order projection decomposition method. Journal of Computational Physics, 206, 252–276.
10. Adam, Y. (1975). A Hermitian finite difference method for the solution of parabolic equations. Computers and Mathematics with Applications, 1, 393–406.
11. Brüger, A., J. Nilsson, andW. Kress (2005). A Compact higher-order finite difference method for the incompressible Navier-Stokes equations. Journal of Scientific Computing, 17(1-4), 551–560.
12. Chorin, A. J. (1968). Numerical solution of the Navier-Stokes equations. Mathematics of Computation, 22(104), 745–762.
13. Christie, I. (1985). Upwind compact finite difference schemes. Journal of Computational Physics, 59, 353–368.
14. Kreiss, H. O., Methods for the approximate solution of time dependent problems. GARP Report No.13,Geneva, 1975.
15. Demuren, A. O., R. V. Wilson, and M. Carpenter (2001b). Higher-order compact schemes for numerical simulation of incompressible flows, Part II: Applications. Numerical Heat Transfer, Part B, 39, 231–255.
16. Dennis, S. C. R. (1989). Compact h4 finite-diffeerence approximations to operators of Navier-Stokes type. Journal of Computational Physics, 85, 390–416.
17. Sengupta, T. K., G. Ganeriwal, and S. De (2003). Analysis of central and upwind compact schemes. Journal of Computational Physics, 192, 677–694.

AUTHORS PROFILE

E. Dhananjaya, Research Scholar, Jawaharlal Nehru Technological University Anantapur, Anantapuramu. He completed his Master of Technology in Industrial Mathematics & scientific Computing From Indian Institute Of Technology, Madras (IIT Madras). He also qualified National Level Examinations Like GATE, CSIR.. He is working as lecturer in Mathematics, Government Model Residential Polytechnic, Madanapalle, Andhra Pradesh.

R. Bhuvana Vijaya, Completed her Doctoral programme in Sri Krishnadevaraya University. She has many numbers of International and National Journals. She is presently working as Professor and Head, department of Mathematics, JNTU college of Engineering, Ananthapuramu.